Asian Journal of Pharmaceutical Sciences 16 (2021) 612–622

Available online at www.sciencedirect.com

ScienceDirect

journal homepage: www.elsevier.com/locate/AJPS

Original Research Paper

Enhanced delivery efficiency and sustained release of biopharmaceuticals by complexation-based gel encapsulated coated microneedles: rhIFNα-1b example

Zequan Zhou[a,b], *Suohui Zhang*[a,c], *Guozhong Yang*[c], *Yunhua Gao*[a,b,c,*]

[a] *Key Laboratory of Photochemical Conversion and Optoelectronic Materials, Technical Institute of Physics and Chemistry, Chinese Academy of Sciences, Beijing 100190, China*

[b] *University of Chinese Academy of Sciences, Beijing 100049, China*

[c] *Beijing CAS Microneedle Technology Ltd, Beijing 102609, China*

ARTICLE INFO

Article history:
Received 10 March 2021
Revised 6 May 2021
Accepted 22 May 2021
Available online 26 June 2021

Keywords:
Coated microneedle
Drug delivery system
Sustained release
Interferon alpha 1b
Sodium alginate

ABSTRACT

Coated microneedles (MNs) are widely used for delivering biopharmaceuticals. In this study, a novel gel encapsulated coated MNs (GEC-MNs) was developed. The water-soluble drug coating was encapsulated with sodium alginate (SA) *in situ* complexation gel. The manufacturing process of GEC-MNs was optimized for mass production. Compared to the water-soluble coated MNs (72.02% ± 11.49%), the drug delivery efficiency of the optimized GEC-MNs (88.42% ± 6.72%) was steadily increased, and this improvement was investigated through *in vitro* drug release. The sustained-release of BSA was observed *in vitro* permeation through the skin. The rhIFNα-1b GEC-MNs was confirmed to achieve biosafety and 6-month storage stability. Pharmacokinetics of rhIFNα-1b in GEC-MNs showed a linearly dose-dependent relationship. The AUC of rhIFNα-1b in GEC-MNs (4.51 ng/ml·h) was bioequivalent to the intradermal (ID) injection (5.36 ng/ml·h) and significantly higher than water-soluble coated MNs (3.12 ng/ml·h). The rhIFNα-1b elimination half-life of GEC-MNs, soluble coated MNs, and ID injection was 18.16, 1.44, and 2.53 h, respectively. The complexation-based GEC-MNs have proved to be more efficient, stable, and achieve the sustained-release of water-soluble drug in coating MNs, constituting a high value to biopharmaceutical.

1. Introduction

Biologics have gradually entered the mainstream of modern medicine research with the rapid development of biopharmaceuticals. Interferon (IFN), a type of host-derived protein, has been systematically described and clinically applied for decades [1]. The subtype IFNα1b is the first IFN recombined and commercialized in China (rhIFNα-1b), which cloned the gene from healthy Chinese cord blood leukocytes

* Corresponding author.
E-mail address: yhgao@mail.ipc.ac.cn (Y.H. Gao).
Peer review under responsibility of Shenyang Pharmaceutical University.

https://doi.org/10.1016/j.ajps.2021.05.002

[2]. It was extensively studied for the antivirus treatment of RSV [3], HBV [4-6], and SARS-CoV [7] as well as antitumor treatment [8-10]. Considering that frequent injections cause a burden to patients during rhIFNα-1b treatment, it is essential to develop a non-invasive administration. At present, numerous studies have been carried out in the field of non-invasive/painless alternative delivery routes, including buccal, oral, and transdermal delivery [11]. Although proteolytic degradation and poor permeability have been improved by co-formulation/modification with protease inhibitors [12], mucoadhesive nanoparticles [13], liposomes [14], etc., their limited transportability and instability indicate that the injection route is still indispensable. Specifically, compared to the success of technical tools in extending half-life, the development of non-invasive biomedicine administration techniques remains a primary challenge [15].

Microneedles (MNs), micron-scale analogue of serological needles, have promising properties including efficient drug delivery, no bleeding, virtually painless, and self-administrative [16], thus exhibiting tremendous potential to substitute intradermal/ subcutaneous injection [17]. Among the variations of MNs, considering the theoretically maximized delivery efficiency and feasibility of industrialization [18], drug-coated MNs are widely used for delivering biologics [19]. In the biologics drug delivery research, coated MNs release drugs in a rapid manner that increases the risk of side effects derived from the wide fluctuation of drug concentration in blood, requiring the need for long-acting coated MNs. However, the long-acting coated MNs system has a technical gap that yet has to be solved. Referring to the well-studied long-acting MNs systems that have been developed so far [20], two types of materials which help in sustained release of drugs can be included in further discussion. Implantable/injectable depots system based on biodegradable polymers (for example, PLGA) [21, 22] is available to achieve sustained release, but unsuitable for hydrophilic biomedicine due to limited drug loading [23] and drug instability [24]. The other type of material, hydrophilic cross-linked/crystallised biocompatible polymer, is acceptable in delivering biologics, which could control the drug release rate by degradation/slow dissolution and avoid denaturation of biologics in organic solvents [25-27]. However, the burden of polymer degradation and risk of material accumulation in the body cannot be ignored [28, 29].

Herein, a gel encapsulated coated (GEC) MNs system was developed: A coated MNs system gradually delivers biopharmaceuticals with a negligible amount of complexation cross-linked material. The implantable coating of GEC-MNs comprised cross-linked gel layers and a medicated water-soluble film encapsulated by gel layers. When inserting the GEC-MNs into the skin, the gel encapsulation absorbed interstitial fluid, depositing the coating from the MNs matrix [30]. The drug coating released the drug with a rate decreased by the outer gel encapsulation. Finally, the drug was completely released during the disintegration of cross-linked encapsulation over time (Fig. 1A). The gel coating was the *in situ* complexation gel that comprised SA and GDL/EDTA-Ca (Fig. 1B). The biocompatible SA *in situ* gel has a controllable period of gelation time, allowing the dip-coating procedure for the fabrication of coated MNs [31-33], and realize the sustained-release of hydrophilic drugs in coated MNs. In the following experiments, the structure of coating was characterized after confirming the manufacturing details. The analysis primarily focused on the positive role of coated gel encapsulation, helping in enhanced drug delivery and stability, and prolonged release of rhIFNα-1b.

2. Materials and methods

2.1. Materials and animals

The rhIFN$\alpha-$1b concentrate was supplied by Tri-Prime Gene Pharmaceutical (Beijing, China). L-polylactide (L-PLA, brand REVODE101) was obtained from Hisun Biomaterials (Zhejiang, China). Medicinal excipient grade sodium alginate (SA, MW approximately 100 000) was purchased from Haizhilin Biotechnology Development (Tsingtao, China). EDTA-Ca was purchased from Solarbio (Beijing, China). Chemically pure GDL was purchased from Alfa Aesar (Heysham, England). Medicinal excipient grades PVA (MW approximately 30,000) was purchased from Nihon Kagaku Sangyo (Tokyo, Japan). Trehalose (dehydrate) was purchased from Hayashibara (Okayama, Japan). Polydimethylsiloxane (PDMS, Sylgard 184) was obtained from Dow Corning (Midland, MI, USA). *Ex vivo* porcine cadaver skin was purchased from Kaikai Science and Technology Trading. The IFNα ELISA assay was purchased from Solarbio (Beijing, China).

Male Sprague Dawley (SD) rats (7 weeks old, 200 ± 15 g) were purchased from SPF Biotechnology (Beijing, China). Rats were housed under specific pathogen-free conditions. Procedures for animal studies were approved by the Institutional Animal Care and Utilisation Committee of the Technical Institute of Physics and Chemistry, CAS. Animal experiments followed the Guide for the Care and Use of Laboratory Animals (Eighth edition, 2011).

2.2. Fabrication of GEC-MNs

2.2.1. Coating solution

Two types of coating solution were used in the fabrication of gel encapsulated coated MNs (GEC-MNs), including a drug coating solution and gel coating solution. The drug coating solution contained drugs, PVA, and trehalose, where PVA and trehalose were added with a mass ratio of 2:1 and its total solid content is provided in subsequent experiments. The gel coating solution was an *in situ* complexation gel (before completing gelation) blended with 2% (wt%) SA and GDL/EDTA-Ca at a ratio of 10:1 (v/v) (except for special instructions). The GDL/EDTA-Ca solution consisted of 300 mM GDL and 300 mM EDTA-Ca.

2.2.2. Fabrication

The MNs matrix (700 μm height, 500 μm intervals, 165 tips) was prepared from L-PLA using a micro-moulding method. PDMS mould was covered with L-PLA particles, continually vacuumed, and heated at 200 °C for 30 min. After demoulding. the PLA MNs matrix was treated with UV/O_3 irradiation for sterilization and hydrophilization (Fig. 2A1).

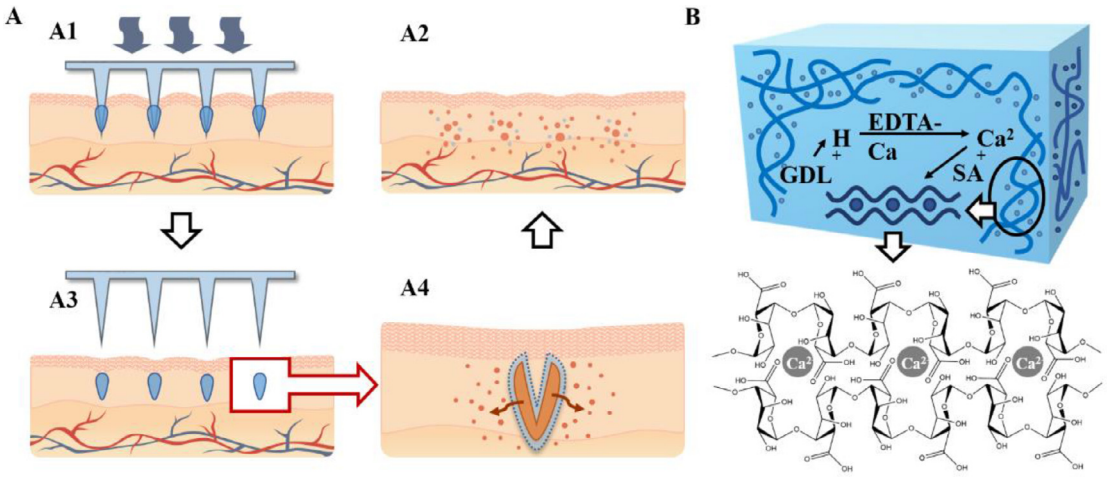

Fig. 1 – Design and concept of rhIFNα–1b GEC-MNs. (A) Hypothetical administration of GEC-MNs. (A1) The GEC-MNs patch is inserted into the skin, and (A2) the coating is implanted in the skin after removing the PLA MNs base. (A3) The drug releases across the outer gel encapsulation. (A4) The gel disintegrates and the drug is released thoroughly over time. (B) SA and GDL/EDTA-Ca hybrid *in situ* complexation gel system. GDL gradually decomposes and releases [H^+], replaces [Ca^{2+}] of EDTA-Ca. The crosslink of [Ca^{2+}] and SA formed homogeneous SA *in situ* gel.

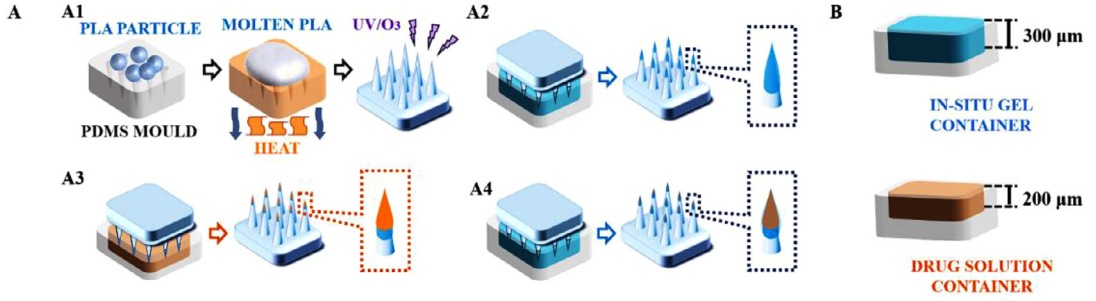

Fig. 2 – Schematic diagram of GEC-MNs fabrication. (A) The procedures to fabricate GEC-MNs were as follows: (A1) production of PLA MNs base, (A2) inner gel encapsulation coating, (A3) drug solution coating, and (A4) outer gel encapsulation coating. (B) The depth of solution containers is 300 μm for SA *in situ* gel and 200 μm for drug solution.

The manufacture of GEC-MNs used a "layer-by-layer" method (Fig. 2A2-2A4). The height of coating solution container was fixed: 300 μm for gel solution and 200 μm for drug solution (Fig. 2B). The first (Fig. 2A3) and last (Fig. 2A4) coating procedure, the formation of inner and outer *in situ* gel coating, were one step before and one step after the implementation of drug coating procedure (Fig. 2A3), respectively. The drug coating procedure would be performed several times. After the above steps were completed, the GEC-MNs patches were dried thoroughly overnight.

2.2.3. *Process optimization*

BSA was used for the process optimization. A bivariate experiment was conducted in which the variables were the solid content of drug coating solution and operating times of drug coating procedure (Fig. 2A3). The formula of drug solution was shown in Table 1. The drug coating procedure was performed 1 to 6 times for each drug solution. The data point was coded in Table 2. The drug loading was quantified using the Brandford method by measuring the BSA concentration of coating-dissolved GEC-MNs in 100 mM trisodium citrate [34].

Table 1 – Drug coating solution formula in the bivariate optimization.

Formula ID	PVA (wt%)	Trehalose (wt%)	BSA (mg/ml)	Viscosity (mPa·s)
I	10	5	10	46.8
II	15	7.5	10	251.5
III	20	10	10	447.2
IV	30	15	10	12 020.0

Table 2 – Data point coding of bivariate experiment.

		Factor B: Coating Steps Operated Times					
		1	2	3	4	5	6
Factor A: Formulation	I	a1b1	a1b2	a1b3	a1b4	a1b5	a1b6
	II	a2b1	a2b2	a2b3	a2b4	a2b5	a2b6
	III	a3b1	a3b2	a3b3	a3b4	–	–
	IV	a4b1	a4b2	a4b3	–	–	–

The delivery efficiency of GEC-MNs patches was examined. The GEC-MNs was inserted into the porcine cadaver skin with the force of 30 N and embedded for 5 min. Then, the MNs patch was peeled off, the remaining BSA (m_x) on the MNs patches was quantified. The delivery efficiency was calculated as follows:

$$\text{Delivery efficiency (\%)} = \frac{m - m_{\times}}{m} \times 100\%$$

Where *m* is the BSA loading of GEC-MNs patches.

After confirming the manufacturing process, change the BSA concentration in the drug solution. The drug loading and the delivery efficiency of the GEC-MNs patches were quantified using the aforementioned method.

2.3. Morphology analysis of GEC-MNs

To visualise the manufacture procedures of GEC-MNs, 0.4% (wt%) trypan blue was added to the *in situ* gel solution; 0.6% (wt%) FITC-BSA was added to the drug solution. The GEC-MNs patch was observed when each step of coating was completed under a stereomicroscope (SMP1000, Nikon, Japan) and optical microscope (BX51, Olympus, Japan).

Structure of the coating layers of GEC-MNs was observed under confocal laser scanning microscopy (CLSM). The *in situ* gel solution comprised 2% (wt%) FITC-SA. The GEC-MNs were imaged using a confocal laser scanning microscope (CLMS, A1RMP, Nikon, Japan), excited at a wavelength of 488 nm. The scanning was stepped 20 μm every time vertically along the Z-axis (direction of the tips towards the platform of MNs), and the reconstructed 3D confocal image of XYZ stack was acquired.

2.4. In vitro drug release

The drug release behaviour in GEC-MNs was studied by plotting the *in vitro* release curves of BSA GEC-MNs with different gel formulation. The *in situ* gel was composed of 2% (wt%) SA and 300 mM GDL/EDTA-Ca, blending at a ratio of 40:1, 20:1, and 10:1 (v/v). The GEC-MNs were enclosed in a 100 kDa dialysis bag and suspended in an Erlenmeyer flask filled with phosphate-buffered saline (PBS) (pH = 7.4). The PBS was magnetically stirred at a speed of 280 rpm and was placed in a 37 ± 1 °C water bath. The samples were collected from the release medium at a predetermined time and supplemented with fresh medium [21].

2.5. In vitro permeation studies trough pig skin

Vertical Franz diffusion cells [35] with 2.7 ml receptor capacity and 0.785 cm^2 surface area were used in the study (system 912-SCT-S; Logan Instruments Corp, Somerset, NJ). The Bama minipig skin specimens were trimmed to a thickness of 800 μm, and mounted in the Franz diffusion cell with the SC side facing the donor compartment. The BSA GEC-MNs patch was fixed to the skin for 5 min. The receptor compartment was filled with 2.7 ml of PBS solution which was continuously stirred with a small magnetic bar and thermostated at 37 ± 1 °C. All the samples in the receptor compartment was collected at predetermined time points and replaced with an equal volume of fresh medium.

2.6. Feasibility and biosafety of in vivo administration

The rhIFNα−1b GEC-MNs patch was applied to the rat abdomen for 5 min after removing the abdominal hair using an animal razor and hair removal cream under pentobarbital anaesthesia (40 mg/kg). After the SD rat was euthanized, the skin with applied GEC-MNs was collected. The skin samples were fixed with 4% paraformaldehyde at 4 °C. Then, the fixed tissues were embedded in paraffin and sectioned at a thickness of 4 μm. The paraffin sections were stained with H&E (Solarbio, Beijing) and scanned under a Pannoramic 250 Flash System (3DHISTECH, Hungary).

Skin irritation was evaluated to study the biosafety of rhIFNα−1b GEC-MNs. Following the above description of GEC-MNs patch administration, the skin site was macroscopically observed at predetermined times for 72 h.

2.7. Stability of rhIFNα−1b GEC-MNs

The rhIFNα−1b GEC-MNs were kept under 25 °C/60% RH and 40 °C/75% RH for 1, 2, 3 and 6 months, respectively. Before the test, the MNs patches were carefully sealed and packaged. The structural stability of rhIFNα−1b in GEC-MNs was determined using the ELISA assay. For the antivirals activity of rhIFNα−1b in the GEC-MNs patches was determined using the vesicular stomatitis virus (WISH-VSV) assay system. WISH cells were seeded in 96-well plates at a density of 2×10^4 cells/well and cultured overnight in a 37 °C, 5% CO_2 incubator. The cells were incubated with successive 4^0- to 4^9- fold dilutions of collected solution of GEC-MNs patches, 1000 IU/ml rhIFNα−1b (as the standard) for 24 h before being challenged with 100 $TCID_{50}$ of VSV. Following 24 h incubation, the cells was stained with crystal violet and its absorbance was measured at 570 nm.

2.8. Pharmacokinetic analysis of rhIFNα−1b GEC-MNs

Experimental animals were randomly assigned into five groups ($n = 6$): GEC-MNs patches with high (40.52 ± 0.92 μg, GEC-MNs-H), middle (20.26 ± 0.46 μg, GEC-MNs-M), and low (10.13 ± 0.23 μg, GEC-MNs-L) rhIFNα−1b loading. The rhIFNα−1b soluble coated MNs group (10.17 ± 0.82 μg, MNs-L) and ID injection group (10 μg, ID injection) were set as the control group.

Blood samples of animals were collected at 0, 0.5, 1, 2, 4, 6, 8, 10, 24, 48 and 72 h after dosing. Venous blood (500 μl) was drawn by tail vein incision. Serum samples were prepared via centrifuging the blood samples at 3000 rpm for 10 min at 4 °C and stored at −20 °C. Finally, the cohort of rats has euthanized 72 h after the rhIFNα−1b application. The serum rhIFNα−1b level was assayed by ELISA kit. The data was calculated by curve-fitting with DAS software package (Shanghai, China, version 3.0) using non-compartmental analyses. The normalized relative bioavailability (F_{rel}) of GEC-MNs/soluble coated MNs (x) was calculated as follows:

$$F_{rel}(x)\ (\%) = \frac{AUC_x \times dose_{ID}}{AUC_{ID} \times dose_x} \times 100\%$$

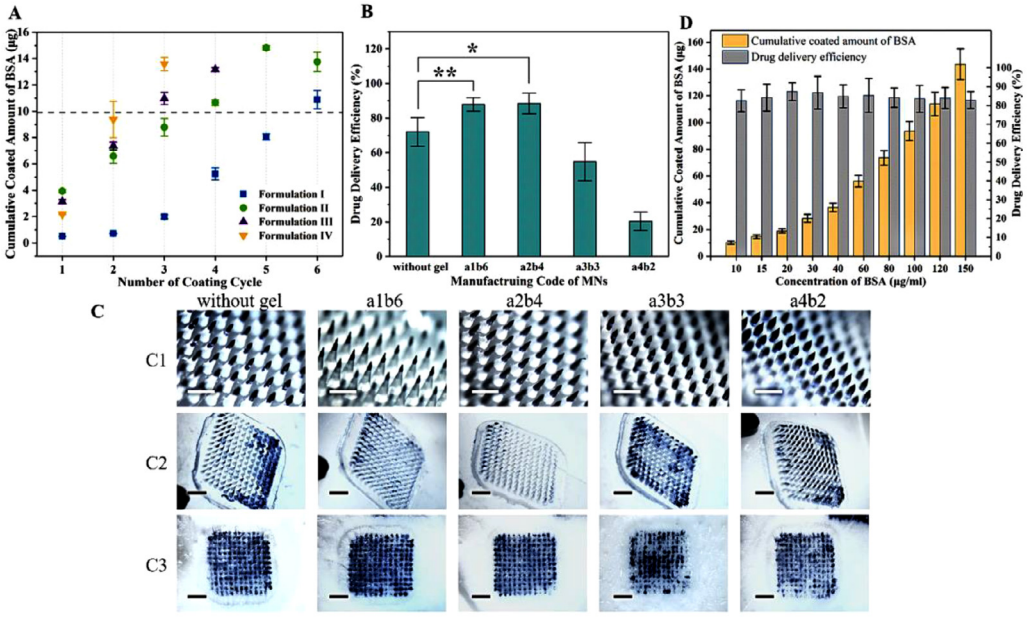

Fig. 3 – Optimization of GEC-MNs fabrication. (A) Bivariate experiment: drug loading of GEC-MNs made by different drug coating formulations and different dug coating cycle. (B) Drug delivery efficiency of the selected GEC-MNs. (C) (C1) MNs with scale bars representing 400 μm. (C2) MNs after administration and (C3) the corresponding skin with scale bars representing 2 mm. (D) Drug loading and delivery efficiency of the GEC-MNs coated with different BSA concentration of drug coating solution. Each point represents the mean ± SD ($n = 6$).

2.9. *Statistical analysis*

Independent experiments were run for at least three samples, and the results are shown as the means ± SD. The statistical significance of the differences was calculated using two-tailed unpaired Student's *t*-test and one-way analysis of variance (ANOVA) or two-way ANOVA, which was performed using Microsoft Excel 2016 software. Values of $P < 0.05$ ($^{*}P < 0.05$, $^{**}P < 0.01$, $^{***}P < 0.001$) were considered as statistically significant.

3. Results and discussion

3.1. *Fabrication of GEC-MNs*

Manufacturing details of GEC-MNs were established from two performances: drug loading and drug delivery efficiency. Drug loading is positively related to the solid content (viscosity) of drug coating solution and number of coating (Fig. 2A3). The commercially rhIFNα−1b is 10, 20,…, 50, 60 μg. Therefore, according to the base number of doses commonly used in clinical, when taking the drug loading 10 μg as the reference standard (Fig. 3A), the GEC-MNs coded with a1b6, a2b4, a3b3, and a4b2 were selected, where the BSA loading was 10.88 ± 1.38, 11.32 ± 0.70, 10.97 ± 0.90 and 9.37 ± 3.01 μg, respectively ($P > 0.05$). Drug delivery efficiency of the selected GEC-MNs patches was 87.87% ± 4.41%, 88.42% ± 6.72%, 54.81% ± 20.04% and 20.38% ± 25.71% (Fig. 3B and 3C). The sharpness of the tips is inversely proportional to the solid content of the drug coating solution. The tips of a3b3 and a4b2 are blunt, resulting in unstable drug delivery efficiency. Compared to the drug delivery efficiency of control (72.02% ± 11.49%), that of GEC-MNs coded with a1b6, a2b4 was statistically higher (a1b6-control, $P = 0.0078$; a2b4-control, $P = 0.019$). Considering the simplification of manufacturing process, the solution formula II and production method of a2b4 were recognized as the production basis for subsequent experiments.

The drug delivery efficiency of GEC-MNs a2b4 (88.42% ± 6.72%) was significantly higher than that of water-soluble coated MNs (72.02% ± 11.49%), indicating that this improvement can be contributed to gel encapsulation. Considering the unavoidable addition of water-soluble carbohydrates as protein stabilizers [36, 37], the gel encapsulation could be considered as a barrier between soluble drug coating and skin moisture. The gel encapsulation prevents the coating from rapidly dissolving during the insertion, and the swelling gel would reduce the drug residue on the PLA matrix by triggering the separation of coating [30].

When the manufacturing process was optimized, the loading of BSA on GEC-MNs was linearly increased (from 10.11 ± 1.28 μg to 143.56 ± 11.43 μg) with the increased concentration of BSA in the drug coating solution (from 10 mg/ml to 150 mg/ml), and the drug delivery efficiency was stable within 82.55% ± 5.86% to 87.37% ± 4.34% ($P > 0.05$) (Fig. 3D). These results indicate that the optimized coating method is controllable in drug loading and have stable drug delivery efficiency, therefore suitable for flexible mass production.

3.2. *Morphology analysis of GEC-MNs*

The coating of GEC-MNs comprised two parts visualised by adding distinct colour components into the corresponding

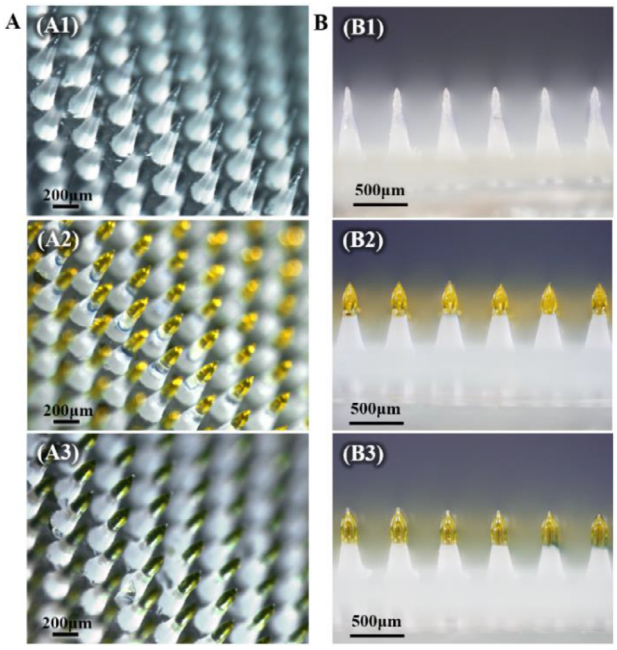

Fig. 4 – Visualisation of GEC-MNs manufacturing process. (A) GEC-MNs on completion of (A1) inner gel encapsulation, (A2) drug coating, and (A3) outer gel encapsulation. (B) Side-view of the corresponding GEC-MNs in production.

solutions (Fig. 4A). When each step of coating was completed, the colour of the tips changed significantly. Obviously, with the completion of outer encapsulation, the height of coating also increased from 200 to 300 μm (Fig. 4B).

To reveal the structure of the multilayer-coating, the GEC-MNs were made using the FITC-SA *in situ* gel and non-fluorescence soluble coating (Fig. 5). At a relative height of 200 to 300 μm, the fluorescence region became intensive comparatively narrow, and gradually disappeared at a height from 300 to 400 μm, indicating that only gel coating was present within this height range. Therefore, the GEC method can control the coating height via varying the depth of coating solution container in the manufacturing process. By observing the sections, it was shown that the *in situ* gel coating was an incompact layer diffusing into the drug coating. The structure of the SA *in situ* gel coating was fluid/non-rigid during the slow progression of the gelation [38, 39]. Although the two coating materials have relative diffusion on the tips, the encapsulated structure was still inferred to be intact (Fig. 5C).

3.3. *In vitro drug release*

To carefully observe the drug release behaviour of GEC-MNs, the *in vitro* release experiment was extended instead of adjusting it for the investigation of *in vivo–in vitro* release correlation. In the extended *in vitro* drug release experiment of 144 h, water-soluble coated MNs (without gel encapsulation) were set as the control group. In the first 12 h, inferring from the slopes, the first point of time when the BSA could be detected in the control, groups of SA *vs.* (GDL/EDTA-Ca) ratios at 40:1, 20:1, and 10:1 (v/v), was 0.5, 5, 5 and 12 h, respectively (Fig. 6B). Compared to the control group, the drug release was delayed when gel encapsulation was involved, verifying the hypothesis described in Section 3.1: the principle of gel encapsulation facilitating drug delivery efficiency. Notably, in the subsequent *in vivo* pharmacokinetics studies, no similar phenomenon of delayed drug release effect was observed.

The cumulative release of BSA in the above-mentioned groups was 91.32% ± 4.33%, 91.09% ± 4.20%, 89.48% ± 3.86%, and 81.11% ± 2.91%, respectively (Fig. 6A). When SA:(GDL/EDTA-Ca) = 10:1 (v/v), *in vitro* cumulative release of BSA was reduced. SA is a polyelectrolyte with a high negative charge density and chemical structure of [–OH] and [–COO^-] [40]. The BSA (isoelectric point 4.7) would be trapped by the undegraded SA gel, and resulting in the decreased cumulative release of BSA. In the subsequent penetration and pharmacokinetic studies, the drug in GEC-MNs was completely released due to the acidic environment and enzymes in the skin [38].

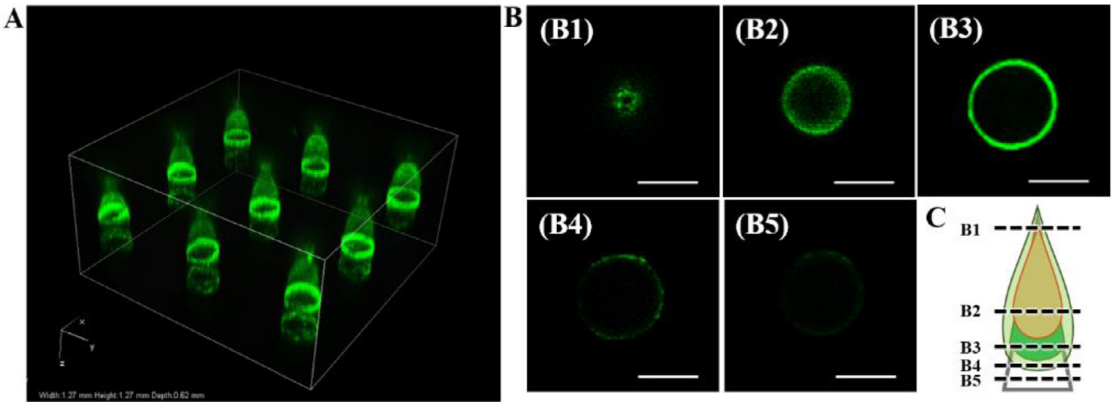

Fig. 5 – CLSM imaging of GEC-MNs coating structure. (A) 3D image of nine implantation sites. (B) Optical sections of the tip at scanning depth: (B1) 100 μm, (B2) 240 μm, (B3) 320 μm, (B4) 440 μm, (B5) 460 μm. Scale bars represent 100 μm. (C) Structural diagram of the coating tip inferred from the CLSM imaging.

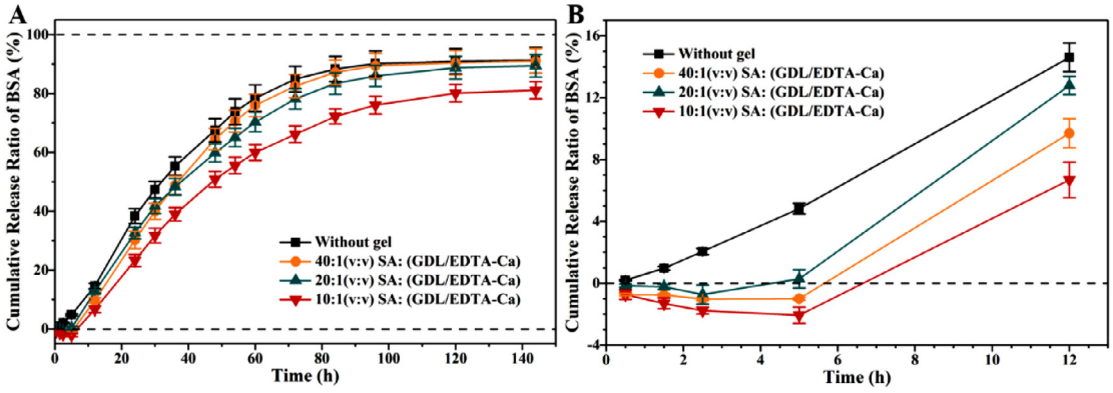

Fig. 6 – Extended *in vitro* release of BSA GEC-MNs with different gel encapsulation formulation at 37 °C. (A) cumulative release ratio of BSA within 0–144 h. (B) The first 12 h of cumulative release ratio of BSA. It was divided into groups of (■) soluble coated MNs, and GEC-MNs with gel encapsulation with SA: (GDL/EDTA-Ca) at a ratio of (●) 40:1; (▲) 20:1; (▼) 10:1 (v/v). Each point represents the mean ± SD ($n = 6$).

3.4. *In vitro permeation studies trough pig skin*

Considering the previous *in vitro* release in terms of the significant slow-release effect of *in situ* gel composed of SA: (GDL/EDTA-Ca) = 10:1 (v/v), the skin permeability study was conducted. The control group was water-soluble coated MNs. In the first 24 h, the cumulative amount of BSA of the control and GEC-MNs were 125.59 ± 9.08 and 49.23 ± 4.59, respectively (Fig. 7B). The permeation rate of the control group was lower than 10 μg/cm^2 from 20 to 120 h. However, in the GEC-MNs group, exhibits an excellent performance over time, mainly from 6 to 96 h. The control and GEC-MNs showed a similar cumulative penetration, which were 137.16 ± 10.27 and 130.99 ± 9.59 ($P > 0.05$) over 5 d, respectively (Fig. 7A). These results clearly show that the GEC-MNs could achieve the sustained-release of the drug.

3.5. *Feasibility and biosafety of in vivo application*

HE-stained skin of the paraffin sections (Fig. 8A) showed two manifestations of micro conduits slice after applying the rhIFNα−1b GEC-MNs. One was the cavity type, extending along the direction from the epidermis to the dermis with a depth of 132.8 – 39.5 μm (Fig. 8A1). In Fig. 8A2, cavities with intact epidermis were observed. The depth range was 137.8–269.6 μm, averaging 202.3 ± 46.3 μm. When the GEC-MNs was inserted into the skin, the elasticity of the skin prevented the tip from penetrating vertically (Fig. 8B), and the height of the embedded tips is greater than the observed vertical height. The coating was inferred to absorb interstitial fluid and collapse 5 min after the GEC-MN administration, without affecting the integral implantation.

Macroscopical epidermal changes of the abdominal skin were periodically observed to evaluate the biosafety of the rhIFNα−1b GEC-MNs administration (Fig. 9). After the removal of the rhIFNα−1b GEC-MNs, the trace of pressing first appeared with no existence of erythema (Fig. 9B1). After 10 min, the indentation slowly becomes flat (Fig. 9B2). After 1 h of removal, slight edema was observed (Fig. 9 B3), and gradually eliminated within 24 h (Fig. 9B4). Moreover, no

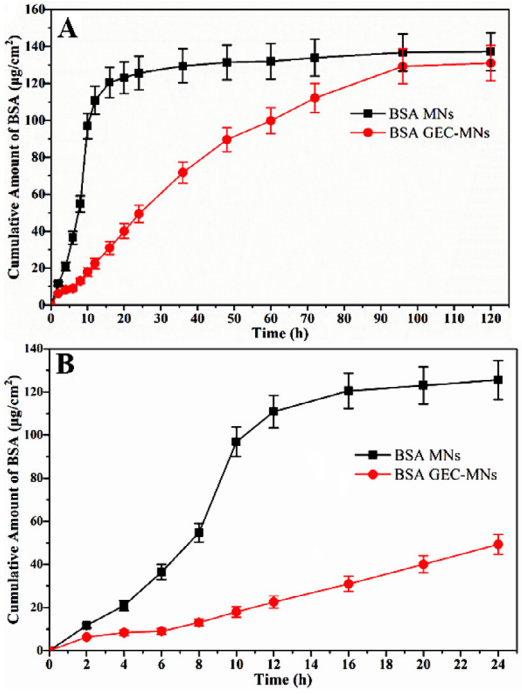

Fig.7 – In *vitro* cumulative permeation of BSA through Bama minipig skin of 800 ± 50 μm thickness at 37 °C. (A) The cumulative permeation of BSA in 120 h and (B) in the first 24 h. It was divided into groups of (■) soluble coated MNs, and (●) GEC-MNs (at loading of 110 μg). Each point represents the mean ± SD ($n = 6$).

further skin irritation was observed within 72 h (Fig. 9B5). To achieve biocompatible GEC-MNs and with sufficient stability of biopharmaceuticals, SA [32, 34] and PVA [41-43] were used as the main materials in this study, which are widely used in tissue engineering and sustained-release delivery research, and acknowledged as biocompatible inactive ingredients. The result of *in vivo* administration verified the biosecurity of rhIFNα−1b GEC-MNs.

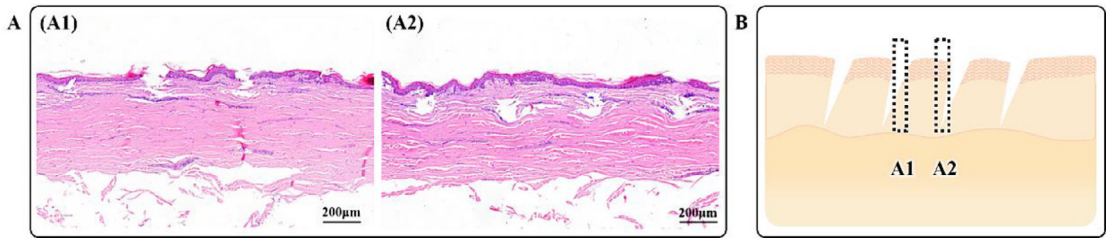

Fig. 8 – Micro conduits sections of the skin after GEC-MNs insertion. (A) The H&E-stained skin sections showed (A1) the cavities extended from epidermis to dermis, (A2) cavities with the intact epidermis. Scale bars represent 200 μm. (B) The diagram inferred from the different tissue morphologies.

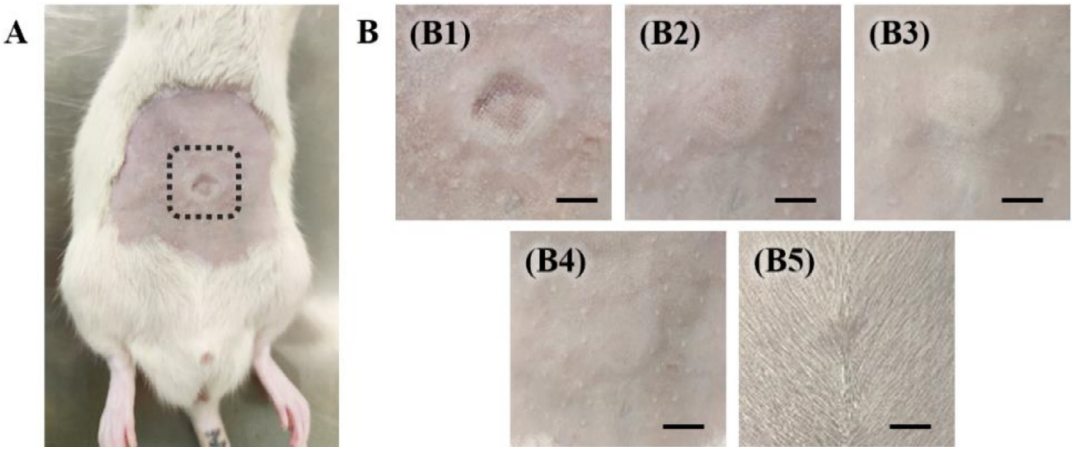

Fig. 9 – Skin irritation after inserting the rhIFNα−1b GEC-MNs. (A) Anaesthetized rat. The dotted line circled the site inserted by rhIFNα−1b GEC-MNs. (B) The skin after inserting the rhIFNα−1b GEC-MNs in time sequence: (B1) immediately, (B2) 10 min, (B3) 1 h, (B4) 24 h, and (B5) 72 h. Scale bars represent 5 mm.

3.6. *Stability of rhIFNα−1b GEC-MNs*

We investigated the storage stability of rhIFNα−1b GEC-MNs (Fig. 10). The experiment was carried out under mild (25 °C/60% RH) and strict (40 °C/75% RH) conditions for 6 months. At 40 °C/75% RH, the recovery rate (0th month: 95.00% ± 3.46%; 6th month: 62.7% ± 7.55%; $p = 0.00091$) and antiviral activity (0th month: $8.08 \times 10^6 \pm 6.54 \times 10^5$ IU/ml; 6th month: $7.94 \times 10^6 \pm 7.99 \times 10^5$ IU/ml; $P = 0.036$) of rhIFNα−1b in GEC-MNs decreased significantly. At 25 °C/60% RH, the rhIFNα−1b in GEC-MNs maintained high structural stability for 6 months (0th month: 90.64% ± 3.07%; 6th month: 84.74% ± 5.46%; $P > 0.05$), and it was the same stability as its antiviral activity (0th month: $7.94 \times 10^6 \pm 5.00 \times 10^5$ IU/ml; 6th month: $7.99 \times 10^6 \pm 8.15 \times 10^5$ IU/ml; $P > 0.05$).

Biopharmaceuticals, including rhIFNα−1b, are usually transported and stored at −4 °C for around 1 month [44; 45]. Both carbohydrates and PVA in GEC-MNs enable to stabilize protein [46]. Under the condition of 40 °C/75% RH, the recovery rate and antiviral activity of rhIFNα−1b in GEC-MNs was stable in the first 3 months. Under the ambient condition (25 °C/60% RH), the rhIFNα−1b could maintain a high level of efficacy for 6 months. Therefore, the rhIFNα−1b GEC-MNs could be stored for a long time at room temperature and humidity, which shows the potential in saving the transportation and storage costs of biological drugs.

Table 3 – Pharmacokinetics parameters of rh-IFNα1b in various administration methods ($n = 6$).

Subject	GEC-MNs			MNs	ID
Dosage (μg)	40.52	20.26	10.13	10.17	10.00
T_{max} (h)	1	1	1	0.5	0.5
C_{max} (ng/ml)	1.18	0.54	$0.28^{***,\#\#\#}$	0.75^{***}	1.30
$T_{1/2z}$ (h)	16.28	15.50	18.16	1.44	2.52
$AUC_{(0-72)}$ (ng/ml·h)	15.86	8.79	$4.18^{\#}$	3.12^{***}	5.04
F_{rel} (%)	78.70	87.21	82.95	61.88	–

Significantly different from ID injection: * $P < 0.05$, ** $P < 0.01$, *** $P < 0.001$.
Significantly different from MNs-L: # $P < 0.05$, ## $P < 0.01$, ### $P < 0.001$.

3.7. *Pharmacokinetics study of rhIFNα−1b GEC-MNs*

Details of pharmacokinetic parameters are shown in Table 3. To compare the differences of GEC-MNs administration with clinical administration, ID injection and water-soluble coated MNs (MNs-L) was set with the rhIFNα−1b dose of 10 μg/rat (Fig. 11A). The C_{max} of rhIFNα−1b of GEC-MNs-L was 0.28 ± 0.09 ng/ml which was lower than MNs-L (0.75 ± 0.11 ng/ml, $P = 0.025$) and ID injection (1.17 ± 0.07 ng/ml, $P = 0.00023$). Additionally, the peak levels (T_{max}) of GEC-MNs-L

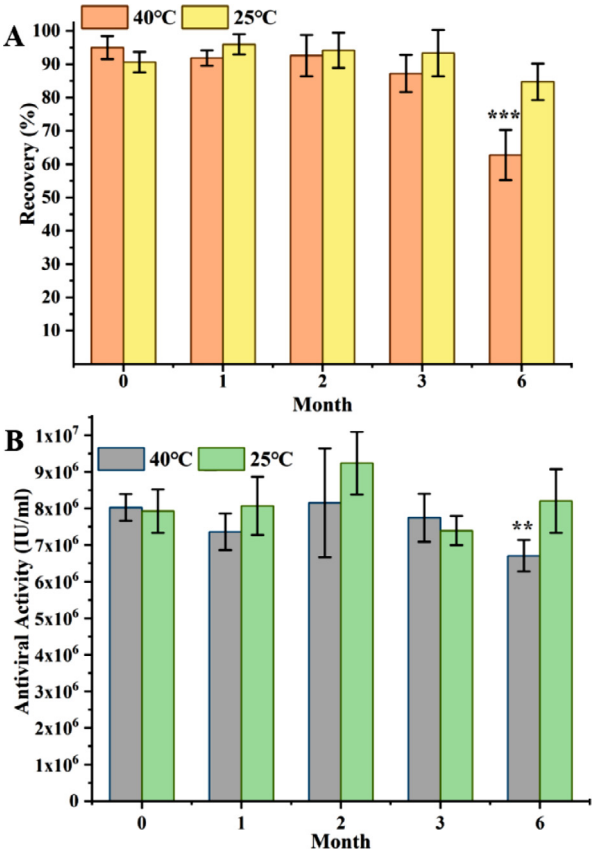

Fig. 10 – Stability of rhIFNα−1b in GEC-MNs at 25 °C/60% RH and 40 °C/75% RH in 6 months. (A) The recovery rate of rhIFNα−1b, and (B) the antiviral activity of rhIFNα−1b (at loading of 10 μg). Each point represents the mean ± SD ($n = 6$).

was delayed for 0.5 h . Furthermore, the serum rhIFNα−1b of GEC-MNs was sustainable for 72 h, while the serum rhIFNα−1b in MNs-L and ID injection failed to be detected at 24 h [47]. The results showed that the transformation into the dosage form of GEC-MNs enables the rhIFNα−1b to achieve a prolonged release from 24 h to 72 h.

The AUC of ID injection was 5.36 ng/ml·h. Setting the AUC of ID injection as the reference, the relative bioavailability (F_{rel}) of MNs-L was 61.88%, while that of GEC-MNs-L was 82.9%. Considering the drug delivery efficiency of 88.42% ± 6.72% shown in Section 3.1, the GEC-MNs had an equivalent efficiency to ID injection, indicating that the gel encapsulation undoubtedly contributed to an enhanced drug delivery efficiency.

To evaluate the dose relationship of GEC-MNs administration, the rats were treated with low (GEC-MNs-L), medium (GEC-MNs-M), and high (GEC-MNs-H) dosage of rhIFNα−1b ($n = 6$) (Fig. 11B). The AUC_{0-72} and C_{max} of GEC-MNs-L, GEC-MNs-M, and GEC-MNs-H showed the dose-dependent linear pharmacokinetics within the dose range of 10.13–40.52 μg. Therefore, the utilisation of GEC-MNs to deliver rhIFNα−1b could comply with the requirements of different doses in clinical.

4. Conclusions

In this study, a complexation-based GEC-MNs model was provided as a long-acting biopharmaceutical transdermal delivery system. The gel encapsulation involves an extremely low amount of complexation-based *in situ* gel, which was necessary to ensure biosecurity. Manufacturing details were optimized for balancing the drug loading and drug delivery efficiency. The drug delivery efficiency of GEC-MNs (88.42% ± 6.72%) was enhanced compared to water-soluble coated MNs (72.02% ± 11.49%). From the results of CLSM scanning, extended *in vitro* release and *in vitro* permeation through the skin, the improved drug delivery efficiency and sustained-release of GEC-MNs was demonstrated. The histological observation and *in vivo* administration of GEC-MNs showed a sufficient insert depth and subtle risk of irritation, confirming the possibility of GEC-MNs for further evaluation. The rhIFNα−1b in GEC-MNs can maintain stable structure and antiviral activity for up to 6 months

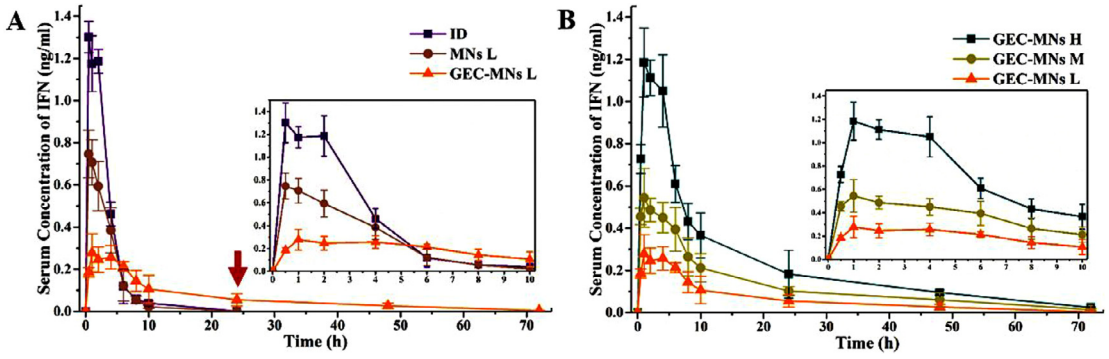

Fig. 11 – Pharmacokinetics profiles of rhIFNα−1b. (A) Curves of dosing rhIFNα−1b in the dosage forms of (■) ID injection, (•) MNs-L and (▲) GEC-MNs-L at dose of 10 μg/rat. The inset shows the curves in the first 10 h. The arrow points to the time when the serum concentration of rhIFNα−1b was lower than LOQ in the groups of ID injection and MNs-L. (B) The curves of GEC-MNs at dosage of (■) 40 μg/rat, (•) 20 μg/rat, (▲) 10 μg/rat. The inset showed the curves in the first 10 h. Each point represents the mean ± SD ($n = 6$).

at 25 °C/60% RH. In pharmacokinetics study, rhIFNα−1b delivered by GEC-MNs was bioequivalent to ID injection (F_{rel} = 82.95%). When gel encapsulation was involved, the drug release prolonged from 24 to 72 h. The AUC_{0-72} and C_{max} of gradient amount of rhIFNα−1b GEC-MNs showed a linear correlation. In conclusion, the GEC-MNs provides a multifunctional, biologically safe drug delivery that achieved a higher efficiency, stability, and sustainable drug release, improving the potential of coated MNs even more from a multiple drugs applicability perspective.

Conflicts of Interest

The authors declare that they have no known competing financial interest or personal relationship that could have influenced the work reported in this manuscript.

Acknowledgments

We thank the Tri-Prime Gene Pharmaceutical Co., Ltd. (Beijing, China) for providing the rh-IFNα−1b. We thank the concentrate Antimicrobial Testing center of the Technical Institute of Physics and Chemistry, CAS for providing the SPF grade animals laboratory.

REFERENCES

[1] Isaacs A, Lindenmann J. Virus interference. I. The interferon. Proc R Soc Lond B Biol Sci 1957;147(927):258–67.
[2] Hussain M, Ni D, Gill D, Liao MJ. IFN-alpha1a gene is the major variant in the North American population. J Interferon Cytokine Res 2000;20(9):763–8.
[3] Chen L, Shi M, Deng Q, Liu W, Li Q, Ye P, et al. A multi-center randomized prospective study on the treatment of infant bronchiolitis with interferon alpha1b nebulization. PLoS One 2020;15(2):e0228391.
[4] XH W, CQ L, XB G, LC F. A comparative study of Phyllanthus amarus compound and interferon in the treatment of chronic viral hepatitis B. Southeast Asian J Trop Med Public Health 2001;32(1):140–2.
[5] Wang CT, Zhang YF, Sun BH, Dai Y, Zhu HL, Xu YH, et al. Models for predicting hepatitis B e antigen seroconversion in response to interferon-alpha in chronic hepatitis B patients. World J Gastroenterol 2015;21(18):5668–76.
[6] Zheng Y, Zhao L, Wu T, Guo S, Chen Y, Zhou T. Efficacy of consensus interferon in treatment of HbeAg-positive chronic hepatitis B: a multicentre, randomized controlled trial. Virol J 2009;6:99.
[7] Duan ZJ, Zhang LL, Xie ZP, Yu ZA, Zhang LP, Zhang B, et al. Anti-SARS virus activities of different recombinant human interferons in cell culture system. Zhonghua Shi Yan He Lin Chuang Bing Du Xue Za Zhi 2003;17(3):205–8.
[8] Masci P, Olencki T, Wood L, Rybicki L, Jacobs B, Williams B, et al. Gene modulatory effects, pharmacokinetics, and clinical tolerance of interferon-alpha1b: a second member of the interferon-alpha family. Clin Pharmacol Ther 2007;81(3):354–61.
[9] Li M, Lu C, Cheng J, Zhang J, Cao C, Xu J, et al. Combination therapy with transarterial chemoembolization and interferon-α compared with transarterial chemoembolization alone for hepatitis B virus related unresectable hepatocellular carcinoma. J Gastroenterol Hepatol 2009;24(8):1437–44.
[10] Gao XM, Zhu Y, Li JH, Wang XY, Zhang XF, Yi CH, et al. MicroRNA-26a induces a mitochondrial apoptosis mediated by p53 through targeting to inhibit Mcl1 in human hepatocellular carcinoma. OncoTargets Ther 2018;11:2227–39.
[11] Bajracharya R, Song JG, Back SY, Han HK. Recent advancements in non-invasive formulations for protein drug delivery. Comput Struct Biotechnol J 2019;17:1290–308.
[12] Brayer SW, Reddy KR. Ritonavir-boosted protease inhibitor based therapy: a new strategy in chronic hepatitis C therapy. Expert Rev Gastroenterol Hepatol 2015;9(5):547–58.
[13] Tran PHL, Tran TTD. Mucoadhesive formulation designs for oral controlled drug release at the colon. Curr Pharm Des 2021;27(4):540–7.
[14] Luo YY, Xiong XY, Tian Y, Li ZL, Gong YC, Li YP. A review of biodegradable polymeric systems for oral insulin delivery. Drug Deliv 2016;23(6):1882–91.
[15] Zelikin AN, Ehrhardt C, Healy AM. Materials and methods for delivery of biological drugs. Nat Chem 2016;8(11):997–1007.
[16] Haq MI, Smith E, John DN, Kalavala M, Edwards C, Anstey A, et al. Clinical administration of microneedles: skin puncture, pain and sensation. Biomed Microdev 2009;11(1):35–47.
[17] Caffarel-Salvador E, Donnelly RF. Transdermal drug delivery mediated by microneedle arrays: innovations and barriers to success. Curr Pharm Des 2016;22(9):1105–17.
[18] Ingrole RSJ, Gill HS. Microneedle coating methods: a review with a perspective. J Pharmacol Exp Ther 2019;370(3):555–69.
[19] Gill HS, Prausnitz MR. Coating formulations for microneedles. Pharm Res 2007;24(7):1369–80.
[20] Chen Z, He J, Qi J, Zhu Q, Wu W, Lu Y. Long-acting microneedles: a progress report of the state-of-the-art techniques. Drug Discov Today 2020;25(8):1462–8.
[21] Zhao X, Zhang S, Yang G, Zhou Z, Gao Y. Exploring trehalose on the release of levonorgestrel from implantable PLGA microneedles. Polymers (Basel) 2020;12(1):59–75.
[22] He M, Yang G, Zhao X, Zhang S, Gao Y. Intradermal implantable PLGA microneedles for etonogestrel sustained release. J Pharm Sci 2020;109(6):1958–66.
[23] Barichello JM, Morishita M, Takayama K, Nagai T. Encapsulation of hydrophilic and lipophilic drugs in PLGA nanoparticles by the nanoprecipitation method. Drug Dev Ind Pharm 1999;25(4):471–6.
[24] Bilati U, Allemann E, Doelker E. Development of a nanoprecipitation method intended for the entrapment of hydrophilic drugs into nanoparticles. Eur J Pharm Sci 2005;24(1):67–75.
[25] Boopathy AV, Mandal A, Kulp DW, Menis S, Bennett NR, Watkins HC, et al. Enhancing humoral immunity via sustained-release implantable microneedle patch vaccination. Proc Natl Acad Sci USA 2019;116(33):16473–8.
[26] Tsioris K, Raja WK, Pritchard EM, Panilaitis B, Kaplan DL, Omenetto FG. Fabrication of silk microneedles for controlled-release drug delivery. Adv Funct Mater 2012;22(2):330–5.
[27] Luo Z, Sun W, Fang J, Lee K, Li S, Gu Z, et al. Biodegradable gelatin methacryloyl microneedles for transdermal drug delivery. Adv Healthc Mater 2019;8(3):e1801054.
[28] Cao S, Tang R, Sudlow G, Wang Z, Liu KK, Luan J, et al. Shape-dependent biodistribution of biocompatible silk microcapsules. ACS Appl Mater Interfaces 2019;11(5):5499–508.
[29] Saravanan M, Bhaskar K, Maharajan G, Pillai KS. Ultrasonically controlled release and targeted delivery of

diclofenac sodium via gelatin magnetic microspheres. Int J Pharm 2004;283(1–2):71–82.
[30] Kim M, Jung B, Park JH. Hydrogel swelling as a trigger to release biodegradable polymer microneedles in skin. Biomaterials 2012;33(2):668–78.
[31] Gao X, Gao L, Groth T, Liu T, He D, Wang M, et al. Fabrication and properties of an injectable sodium alginate/PRP composite hydrogel as a potential cell carrier for cartilage repair. J Biomed Mater Res A 2019;107(9):2076–87.
[32] Han Y, Zeng Q, Li H, Chang J. The calcium silicate/alginate composite: preparation and evaluation of its behavior as bioactive injectable hydrogels. Acta Biomater 2013;9(11):9107–17.
[33] Growney Kalaf EA, Flores R, Bledsoe JG, Sell SA. Characterization of slow-gelling alginate hydrogels for intervertebral disc tissue-engineering applications. Mater Sci Eng C Mater Biol Appl 2016;63:198–210.
[34] Choi JW, Kang E, Kwon OJ, Yun TJ, Park HK, Kim PH, et al. Local sustained delivery of oncolytic adenovirus with injectable alginate gel for cancer virotherapy. Gene Ther 2013;20(9):880–92.
[35] Martins M, Azoia NG, Shimanovich U, Matama T, Gomes AC, Silva C, et al. Design of novel BSA/hyaluronic acid nanodispersions for transdermal pharma purposes. Mol Pharm 2014;11(5):1479–88.
[36] Chu LY, Ye L, Dong K, Compans RW, Yang C, Prausnitz MR. Enhanced stability of inactivated influenza vaccine encapsulated in dissolving microneedle patches. Pharm Res 2016;33(4):868–78.
[37] Mistilis MJ, Bommarius AS, Prausnitz MR. Development of a thermostable microneedle patch for influenza vaccination. J Pharm Sci 2015;104(2):740–9.
[38] Qu B, Chen C, Qian L, Xiao H, He B. Facile preparation of conductive composite hydrogels based on sodium alginate and graphite. Mater Lett 2014;137:106–9.
[39] Hong GP, Chin KB. Evaluation of sodium alginate and glucono-delta-lactone levels on the cold-set gelation of porcine myofibrillar proteins at different salt concentrations. Meat Sci 2010;85(2):201–9.
[40] Qin Y, Cai L, Feng D, Shi B, Liu J, Zhang W, et al. Combined use of chitosan and alginate in the treatment of wastewater. J Appl Polym Sci 2007;104(6):3581–7.
[41] Ivanova NV, Kuzmina ML. Protocols for dry DNA storage and shipment at room temperature. Mol Ecol Resour 2013;13(5):890–8.
[42] Elversson J, Millqvist-Fureby A. Aqueous two-phase systems as a formulation concept for spray-dried protein. Int J Pharm 2005;294(1–2):73–87.
[43] Chu LY, Ye L, Dong K, Compans RW, Yang C, Prausnitz MR. Enhanced stability of inactivated influenza vaccine encapsulated in dissolving microneedle patches. Pharm Res 2016;33(4):868–78.
[44] Schepart BS, Burns BA, Evans S, Poleon GP. Long-term stability of interferon alfa-2b diluted to 2 million units/mL. Am J Health Syst Pharm 1995;52(19):2128–30.
[45] Appenheimer MM, Schepart BS, Poleon GP, Evans SS. Stability of albumin-free interferon alfa-2b for 42 days. Am J Health Syst Pharm 1998;55(15):1602–5.
[46] Cole G, Ali AA, McCrudden CM, McBride JW, McCaffrey J, Robson T, et al. DNA vaccination for cervical cancer: strategic optimisation of RALA mediated gene delivery from a biodegradable microneedle system. Eur J Pharm Biopharm 2018;127:288–97.
[47] Rutenfranz I, Kirchner H. Pharmacokinetics of recombinant murine interferon-gamma in mice. J Interferon Res 1988;8(5):573–80.